

# In silico modeling of emodin's interactions with serine/threonine kinases and chitosan derivatives

Rohit Suresh<sup>1,6</sup>, Srinitya Sriram<sup>2,6</sup>, Vivek Garg<sup>3,6\*</sup>, Yash Kamdar<sup>4,6\*</sup>, Sahana Kuchibhotla<sup>5,6</sup>, Gayathri Renganathan<sup>6</sup>

<sup>1</sup>Lynbrook High School, San Jose, California

<sup>2</sup>Dougherty Valley High School, San Ramon, California

<sup>3</sup>Irvington High School, Fremont, California

<sup>4</sup>Washington High School, Fremont, California

<sup>5</sup>Mission San Jose High School, Fremont, California

<sup>6</sup>Department of Chemistry, Biochemistry, and Physical Science, Aspiring Scholars Directed Research Program, California

\*denotes equal authorship

## SUMMARY

Natural products are quickly gaining relevance as effective anticancer agents, and one example, emodin, possesses inhibitory activity against a broad spectrum of kinases, regulatory enzymes that control biological activity via phosphorylation of other molecules. Herein, through protein-ligand docking, we investigated the effect of the interaction of emodin with serine/threonine kinases, a subclass of kinases that is overexpressed in many cancers, which is implicated in phosphorylation cascades. These cascades act as intracellular messaging systems, and in the case of cancer, modify protein expression in the cell to essentially make it immortal. Thus, competitive inhibition by emodin can reduce the expression of a wide range of proteins required for essential cell function, resulting in cell death. Because the majority of serine/threonine kinases have similar active sites, we have successfully created a blueprint for emodin binding and interactions with active site residues, which include many hydrophobic interactions and minimal amounts of hydrogen bonding. Through molecular dynamics we found that emodin forms favorable interactions with chitosan and chitosan-PEG (polyethylene glycol) copolymers, which could aid in loading drugs into nanoparticles (NPs) for targeted delivery to cancerous tissue. Both polymers demonstrated reasonable entrapment efficiencies, which encourages experimental exploration of emodin through targeted drug delivery vehicles and their anticancer activity.

## INTRODUCTION

Emodin is a natural derivative of anthraquinone, a polycyclic aromatic hydrocarbon derived from anthracene used to manufacture dyes and is typically found in various medicinal plants such as rhubarb, buckthorn, molds, and lichen

(Figure 1) (1). The molecule has various therapeutic roles as a tyrosine kinase inhibitor, a laxative, and an anticancer agent (2). Emodin binds to various proteins with anticancer properties such as serine/threonine kinases, dual specificity kinases, GTPases, and proteases (3–5). Kinases are central to maintaining proper cellular function via turning on protein functions through the phosphorylation of specific amino acids. Serine/threonine kinases act specifically on serine and threonine amino acid residues on regulatory proteins, which leads to widespread effects through phosphorylation cascades. Similarly, dual-specificity kinases act as serine/threonine and tyrosine kinases.

Due to their role in promoting cell proliferation and anchorage-independent growth, the overexpression of the various protein kinases is typically associated with oncogenesis (6). Specifically, overexpression of dual-specificity kinases can cause increased cell proliferation and anchorage-independent growth of cells—critical characteristics for tumor growth and metastasis (7). Thus, protein kinases serve as promising targets for future anticancer venues. The use of polymeric nanoparticles, particles that are 1–500 nm in length, is emerging as a promising method of small molecule delivery in cancer therapeutics due to characteristics like high biocompatibility, broad-structure variety, and bioimitive (imitating biological properties) characteristics (9). Nanoparticles represent one mode through which emodin may be delivered in order to maximize the amount of emodin that enters its target cell. Chitosan, a polysaccharide composed of glucosamine monomers, nanoparticles specifically have several advantages including low toxicity, high biocompatibility and biodegradability, stability, and site-specific drug targeting abilities (10–11). The molecular dynamics (MD) approach makes use of computer simulations to model the movement of molecules at the atomic level. Traditionally, this method has been utilized to model protein-drug complex interactions on a time course but has more recently been used to model nanoparticles and

their interactions with surrounding media. While inorganic nanoparticles and carbon-based nanoparticles have primarily been studied, polymer nanoparticle interactions have not been accurately predicted through the same *in silico* approaches. However, many studies are aiming to overcome this gap in knowledge. In one study exploring the production of solid lipid nanoparticles (traditionally polymer nanoparticles), drug entrapment efficiency was found to be more than 87% and showed long-term physical stability (12). In another study, chitosan nanoparticles were investigated to deliver ciprofloxacin hydrochloride. Drug entrapment efficiency was found to increase with increasing amounts of drug in polymer to drug ratios (13).

Previous studies have investigated the binding mechanisms behind emodin and tyrosine kinase interactions (14). Due to emodin's ability to bind to casein kinases (a type of serine/threonine kinase), we hypothesized that emodin would be able to bind to serine/threonine kinases in general. In this study, the specific characteristics of emodin binding to serine/threonine kinases were identified via a variety of *in silico* methods to aid in identifying emodin's mechanism of action as an anticancer agent. By identifying the specific interactions that would allow emodin to bind to serine/threonine kinases as a general class of proteins, we begin to understand the complex mechanism of action for emodin (15). Furthermore, because emodin consists of a hydrophobic core surrounded by polar (having an electric charge) functional groups, like phenols, we hypothesized that emodin would form strongly favorable interactions with chitosan. These interactions, in turn, would lead to higher entrapment efficiencies at lower drug to polymer ratios that increase as more drug molecules are added. Through investigating this hypothesis, we have optimized one parameter of chitosan nanoparticle synthesis, which is significant because it highlights that the large amounts of trial and error commonly associated with the synthesis of chitosan nanoparticles can be reduced.

## RESULTS

### Molecular docking

In order to model emodin's interaction with various protein classes, we investigated using molecular docking, from which the binding scores between emodin and the different proteins were found. The binding scores described in this section represent the predicted affinity in kcal/mol between emodin and the proteins of interest. We used binding scores to rank the proteins with the intention of identifying those with which emodin had the strongest interaction. Serine/threonine kinases were found to bind well to emodin with binding scores averaging approximately -8.6, in contrast to another emodin-binding protein caspase-3, a cysteine protease, which only scored -5.8. In general, binding in these proteins was facilitated by emodin's nonpolar interactions with the amino acid residues leucine and valine in the active site (Figure 2a). Additionally, binding was also facilitated by hydrogen bonding between the phenols on emodin and the polar

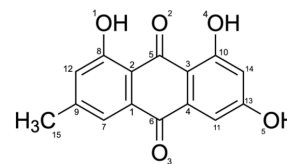


**Figure 1. Chemical structure of emodin.** Emodin is composed of three six-membered carbon rings with three hydroxyl groups, a methyl group, and two carbonyl groups attached. Image generated using ChemDraw molecule editor.

regions of the protein (Figure 1). Dual-specificity kinases did not bind well to emodin due to their differences in polarity; the polar regions of these kinases cannot interact with the nonpolar regions of emodin (Figure 2b). When bound to MAPK-9 and S/THPK (two kinases included in the molecular docking studies), emodin was found to interact with various residues including leucine, valine, glycine, phenylalanine, and threonine (L275, V158, G226, F222, and T293 in MAPK-9; L154, V38, G31, and F35 in S/THPK) (Figure 2c-2d). Proteins with low-magnitude binding scores did not display specificity to any amino acid residues. Overall, proteins with high-magnitude binding scores had interactions with emodin primarily via leucine and valine residues. Specific proteins used are identified in Table 1. Additionally, emodin was found to bind to serine/threonine kinases in the same location as the adenosine of ATP as opposed to where the triphosphate binds

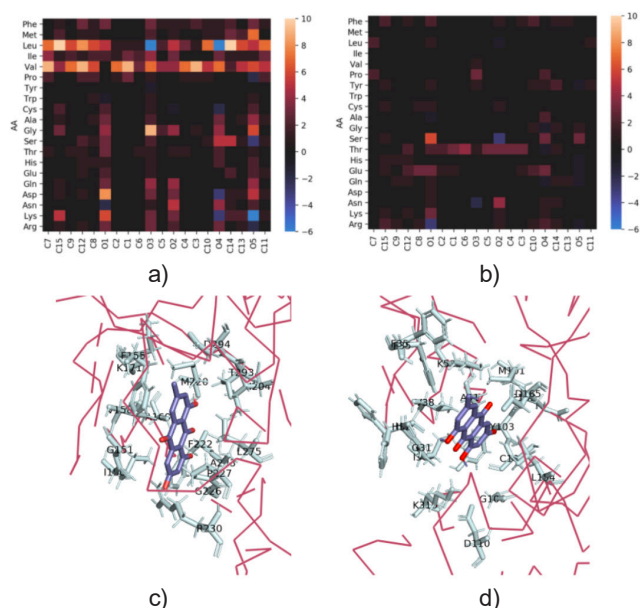


**Figure 2. Residues interacting with emodin.** Heatmap of residues interacting with emodin in (a) serine/threonine kinases and (b) dual specificity kinases. Positive values signify nonpolar interactions while negative values signify polar interactions like hydrogen bonds. The magnitude of values represents the number of interactions of that specific type occurred over all structures within the class of the heatmap. (c) Residues within 4 Å of emodin in MAPK-9. (d) Residues within 4 Å of emodin in S/THPK.

Table 1. Names and class of protein targets emodin was bound to during docking.

Protein Name	Protein Class	PDB ID	PDB ID for Protein-Drug Complex (16)	Score for Emodin
MEK1 (17)	dual specificity kinase	3E8N	3E8N	-9.8
MAPK-9 (18)	serine/threonine kinase	3DTC	3DTC	-9.7
S/THPK (19)	serine/threonine kinase	6BDN	6BDN	-9.7
MAPK-10 (18)	serine/threonine kinase	2B1P	2ZDU	-9.6
MAPK-12 (18)	serine/threonine kinase	5CEN	5VO2	-9.5
MAPK-2 (18)	serine/threonine kinase	3R2B	3KGA	-9.3
PIM-1 (20)	serine/threonine kinase	3C4E	3C4E	-9.2
PI3K (21)	serine/threonine kinase	3APC	1E7V	-9.1
MTOR (22)	serine/threonine kinase	5FLC	5FLC	-8
PRK1 (23)	serine/threonine kinase	4OTD	4OTI	-8.5
RAC1 (24)	serine/threonine kinase	1HH4	4GZM	-7.4
Casein kinase 2 (25)	serine/threonine kinase	4MD7	4GRB	-6.6
MAPK (26)	serine/threonine kinase	3S4E	4BID	-6.5
Aryl hydrocarbon receptor (27)	transcription factor	5NJ8	5V35	-8.3
MAP2K-4 (18)	dual specificity kinase	3VUT	3ALN	-7.8
DSP-7 (28)	dual specificity kinase	6IB0	6IB0	-7.8
VEGFR (29)	tyrosine kinase	2VPF	4AGC	-7.9
HSP90 (30)	kinase regulator	1US7	2QF6	-7.8
MTH1 (31)	pyrophosphatase	5OTM	5MZG	-7.8
Bcl-2 Protein (32)	antiapoptotic protein	7CA4	4AQ3	-7.6
Topoisomerase (33)	topoisomerase	1LPQ	1SEU	-7.5
Ras Protein (34)	atpase	4M21	1X1R	-7.2
Matrix metalloproteinase-2 (35)	proenzyme	1CXW	1HOV	-5.9
Caspase-3 (36)	cysteine protease	3KJF	3KJF	-5.8

(Figure 3). ATP plays a key role in many cellular processes by providing energy to fuel chemical reactions. Consequently, it can play a role in intracellular signaling pathways involved in the suppression and activation of tumor suppressor and activators. Due to emodin competing with ATP to bind to the kinase, downstream effects of serine/threonine kinases such as cell proliferation and differentiation may be blocked.

### Molecular dynamics

We chose to run MD on MAPK-9 because it had the most negative binding score, which prompted further investigation into whether emodin can remain stable in the protein rather than temporarily binding strongly. Emodin remained stable in the binding pocket of MAPK-9 throughout the 1 ps simulation (Figure 4). This was enough time to allow the protein to stabilize and see the difference between emodin and native bound states. Additionally, the backbone of the protein structure was more stable in the presence of bound emodin compared to its native state bound to ATP. Consequently, emodin would be an effective inhibitor as the protein was stabilized when emodin was bound, as it is more thermodynamically

favorable, which means it is less reactive, than its unbound state. Furthermore, this indicates that emodin would likely form competing interactions with the protein relative to ATP, the native substrate.

The fourth and fifth oxygen of emodin (located on the third carbon ring) are closest to MAPK-9 when bound, within a range of 3.6–4.0 Å, whereas the first, second, and third oxygens range from 5.2–7.0 Å away. The carbons of

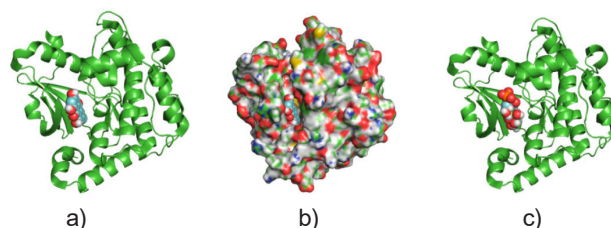
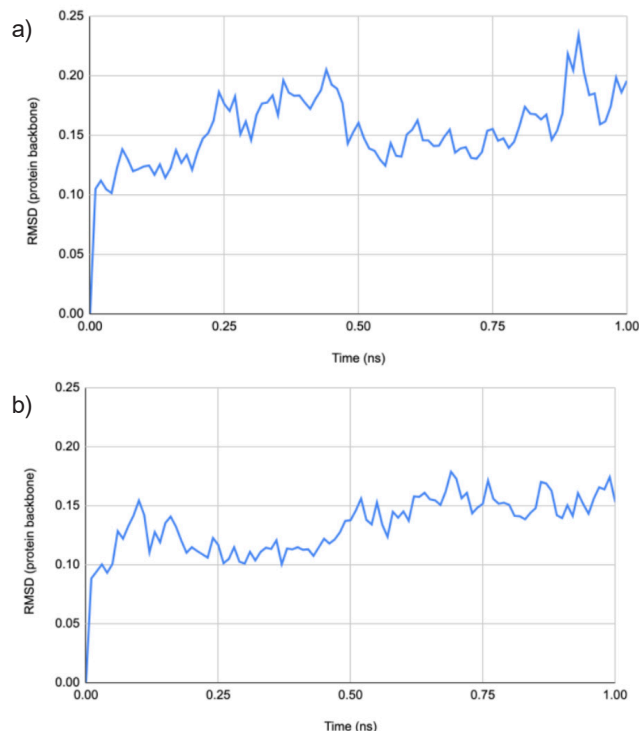


Figure 3. Emodin bound to S/THPK. (a) and (b) S/THPK bound to only emodin. (a) depicts PyMol's ribbon model of S/THPK bound to emodin. (b) depicts PyMol's surface model of S/THPK bound to emodin. (c) S/THPK bound to emodin and ADP.



**Figure 4. RMSD of the protein backbone of MAPK-9 over 1 ns. (a)** RMSD fluctuations of the MAPK-9 backbone free protein (control). **(b)** RMSD fluctuation of the MAPK backbone with emodin present.

emodin are facing toward the solvent, while the oxygens and hydrogens are interacting with MAPK-9 through hydrogen-bonding (**Figure 5**). The purpose of modeling emodin's location in relation to MAPK-9 was to further understand how the molecule interacts with the protein.

When studying the emodin and polymer interactions, in both the chitosan and chitosan-PEG (copolymer) MD trials, a clear maximum entrapment efficiency (EE) occurred at a drug:polymer ratio of 0.4. Overall, the copolymer trials had lower EEs compared to those with chitosan. Specifically, the chitosan NP had a maximum EE of 65.7% while the copolymer NP was 60.9%, and this trend was consistent throughout most of the drug:polymer ratios. Furthermore, there was not a linear relationship between the drug:polymer ratio and EE, which was contrary to our hypothesis; instead, the EE quickly climbed to a maximum as the ratio was increased, then slowly decreased to a plateau (**Figure 6**). **Equation 1** was chosen to model the initial increase in EE and the plateau that followed.

Downstream PyMOL analysis, a protein visualization pipeline, indicated that emodin relies on both hydrogen bonding and hydrophobic interactions to remain near the chitosan. This finding is consistent with emodin's structure, as it has a hydrophobic anthraquinone core surrounded by phenols. Thus, the core participates in hydrophobic interactions, while the polar phenols and ketones form hydrogen bonds with the polar alcohols and amines on chitosan (**Figure 7**).

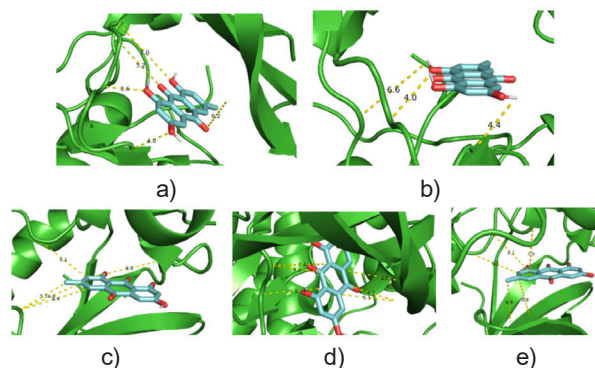


**Figure 5. Position of molecular components of emodin relative to MAPK-9.** The **(a)** oxygens on emodin and MAPK-9, **(b)** hydrogens on emodin and MAPK-9, **(c)** carbons in the 1st ring of emodin and MAPK-9 **(d)** carbons in the middle ring of emodin and MAPK-9, and **(e)** carbons in the 3rd ring of emodin and MAPK-9 are all closely located to the protein.

## DISCUSSION

The docking studies that we presented within this work showed that emodin is capable of binding to a wide variety of serine/threonine kinases due to the presence of a nonpolar binding pocket, which is assisted by hydrogen bonding. Because emodin has the potential to act as a competitive inhibitor to ATP, it suppresses serine/threonine kinase activity by inhibiting the phosphorylation of protein substrates (37). Despite this, emodin is unable to strongly bind in the pocket of dual-specificity kinases, which also use ATP as their source of phosphate for phosphorylation, because their pockets contain more polar residues. Our results also show that there is a lack of nonpolar residues since dual-specificity kinases have binding and allosteric sites primarily lined with polar amino acids. Nonpolar residues are essential for emodin binding to serine/threonine kinases, further supporting that emodin could not form stable interactions with dual specificity

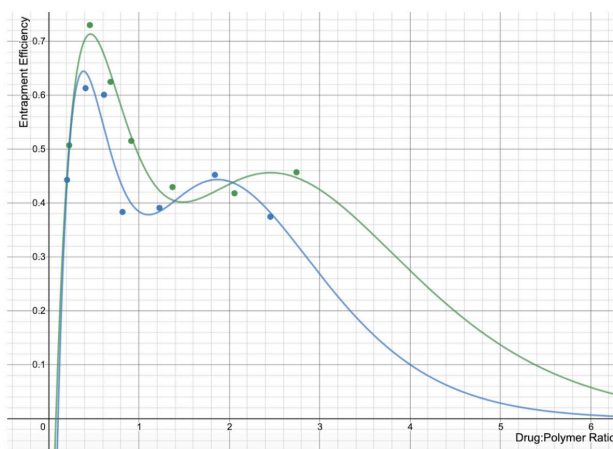


**Figure 6. EE of chitosan (green) and chitosan-PEG NP (blue).** The equation showed reasonable correlation coefficients of 0.9972 and 0.8857, respectively.

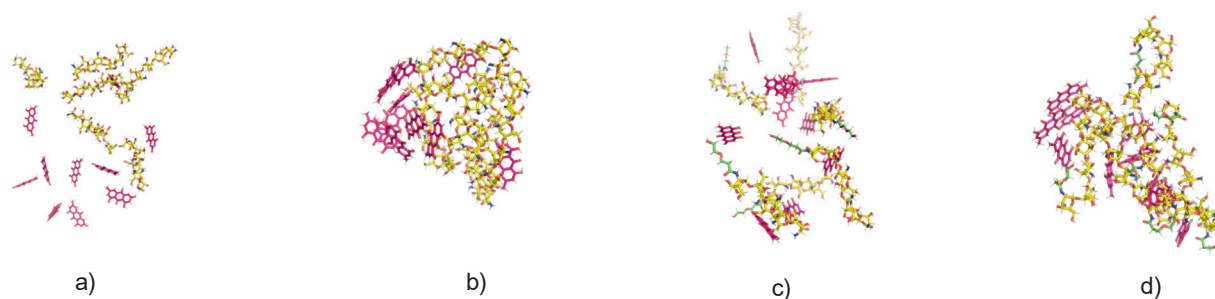


**Figure 7. Chitosan and Chitosan-PEG system in MD simulation.** Chitosan system (a) before and (b) after MD simulation. Chitosan-PEG system (c) before and (d) after MD simulation.

kinases. Kinases typically function at upstream levels of signal transduction pathways; therefore, inhibition affects a multitude of downstream functions at the molecular level, which results in the cell no longer being able to sustain critical functions. Because serine/threonine kinases and tyrosine kinases are both generally overexpressed in tumor cells, a broad-spectrum inhibitor like emodin may be effective in promoting cell death of or preventing cellular proliferation of cancerous cells. However, normal somatic cells also rely on kinase function, highlighting that it is important to develop alternative formulations that minimize off-target effects.

We have successfully demonstrated that emodin can be efficiently loaded into chitosan nanoparticles in order to aid in the targeting of emodin to cancerous tissue. Both regular chitosan and chitosan-PEG polymers peak in EE when the drug:polymer ratio is about 0.4. Our hypothesis relied on the assumption that emodin-polymer interactions were generally favorable, but our experimentation suggests that emodin's interaction with the polymers only leaned to one side of the equilibrium. As a result, not all the emodin molecules interacted with the chitosan at high ratios. During the *in silico* synthesis of NPs, the polymer strands bent around emodin molecules, which increased the number of emodin-polymer interactions. Consequently, at lower drug:polymer ratios, it appears that the EE is more favored for emodin-polymer interactions because fewer emodin-emodin interactions can form, and the formation of interactions is closer to random. As the drug:polymer ratio increases, the EE plateaus and

drops toward 0 due to fewer polymer molecules to interact with emodin. The chitosan-PEG produced a slightly lower EE because emodin was unable to efficiently interact with the PEG, which reduced the amount of polymer available for emodin. PEG is moderately polar due to the ether linkages, but emodin consists of distinct nonpolar and polar regions, which results in unfavorable interactions. Despite this, the EEs between the two polymers were similar, yet the chitosan-PEG polymer increases NP stability, which outweighs the slight loss of EE. Because a small number of monomer units were used in the simulation, all the polymers aggregated together to form the NP, but the PEG in the copolymer moved to the exterior of the NP (**Figure 8**). Consequently, the copolymer adopted a more flexible structure that was able to integrate emodin more thoroughly, while the normal chitosan remained rigid, resulting in the copolymer having an irregular shape and the chitosan creating a spherical NP (**Figure 9**). The irregular shape was more flexible, so it presents a benefit toward incorporating the drug into the nanoparticle as well as increasing nanoparticle-cell membrane interactions. Despite these promising results, our results are solely computational, and so factors such as surfactants and solvents, which are commonly used in nanoparticle synthesis, were not accounted for. This suggests that our study is only an estimate of what laboratory results could produce, and further testing is warranted.

With the use of computational tools including docking and MD, we have supported that emodin effectively binds to a broad spectrum of kinases, showing its potential for cytotoxic activity as it may successfully inhibit the effect protein kinases have in cancerous development. As a result, future studies should investigate the design and testing of serine/threonine kinase specific inhibitors based upon an emodin scaffold. This can be mediated using NPs because chitosan is able to favorably interact with emodin, which will likely lead to a high EE and stable release rate, which can be quickly synthesized and tested in biological solutions. The results of this study showcase that emodin has the potential to be a cancer regulator through kinase inhibition and that it can be delivered through chitosan nanoparticles.

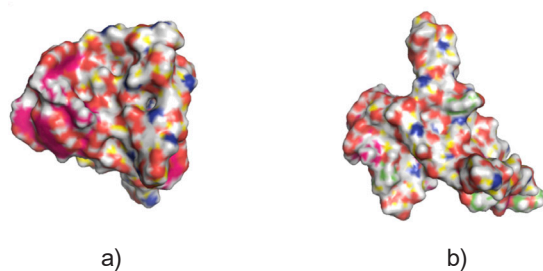


**Figure 8. Surface morphology of nanoparticles.** Surface morphology of (a) chitosan and (b) chitosan-PEG NP.

## METHODS

### Docking

Emodin *in silico* structure was computationally constructed using Avogadro and optimized with the MMFF94 force field for 10,000 steps before being fully optimized with TD-DFT in Orca using the B3LYP and def2-TZVP functionals with CPCM(Water) as the solvent model (38).

Molecular docking is used to study the interactions between two molecular structures using computer simulations. UCSF (University of California San Francisco) Chimera, a molecular visualization tool, was used to construct proteins based on its PDB ID taken from RCSB. All non-standard residues, subunits, and ligands were deleted and emodin was loaded onto the receptor file. The receptor and emodin were prepped prior to performing surface-binding analysis using the Autodock Vina extension on Chimera (39). A box was used to encapsulate the ligand and receptor and blind docking was performed. From the DockViewer, the top binding score was recorded. The binding score was calculated by summing up individual terms such as distance-dependent atom pair interactions (40). The complex was then loaded into PyMOL, another standard molecular visualization tool, to compare with other protein-drug complexes (41).

A PDB ID for the protein in complex with a leading drug was obtained from RCSB. The protein-drug complex was then aligned through PyMOL with the protein-emodin complex. The ligands listed under the small molecules section on the RCSB profile for the protein-drug complex were then highlighted in PyMOL. The binding locations of the selected ligands were compared to the binding location of emodin on the protein.

A script was made using Python to locate all the residues within 2.75 Å of each non-hydrogen atom in emodin. This script was run on all the docked conformations, and a heatmap was created to represent the amino acid frequency near each amino acid for groups of proteins including serine/threonine kinases, dual specificity kinases, and low-scoring proteins (42).

### Molecular dynamics

The docked structure of emodin to MAPK-9 was chosen for further analysis through molecular dynamics (GROMACS version 2020.4) (43). The structure was solvated in water using the TIP3 model, and EM, NVT, NPT equilibration were conducted until the system was stable. Afterwards, a 1 ns simulation was performed, and the RMSD of the backbone chain was plotted over time. This was repeated three times, and the average was used for data generation.

A base polymer of chitosan with 6 monomer units of glucosamine was constructed using Avogadro and optimized with the MMFF94 force field for 10,000 steps. Similarly, to construct the copolymer, the base polymer was taken, and 3 units of polyethylene glycol (PEG) were directly attached onto the amine group of the last glucosamine monomer on chitosan. Parameters for GROMACS were generated through the CHARMM webserver hosted by the University

of Maryland (44–48). Next, a system of six polymers and a predetermined number of emodin molecules were added to a box without water or ions, which has been previously reported to accurately simulate NP formation. An energy minimization (EM) was performed for a maximum of 5,000 steps (49). Afterward, the system was optimized for 75,000 steps under a constant number of molecules, volume, and temperature (NVT) at 300 K. A PME mesh was used in the system and LINCS, a setting available, was used to constrain the bond lengths and hydrogen bonds, which increased the speed of the simulation without a large impact on accuracy. We used a Verlet cutoff scheme, which utilizes exact cutoffs to determine the location of atoms throughout the simulation and to increase the speed of the simulation. For each trial, the run was repeated three times, and the average was used for data generation.

After the simulation was completed, a script was made to find the shortest distance between any atom on emodin and any atom on the nearest chitosan polymer. The number of emodin molecules less than 2.75 Å from chitosan was averaged over the last 25,000 steps of the simulation and divided by the total emodin molecules in the simulation to find the entrapment efficiency (50). After the entrapment efficiency was plotted, **Equation 1** was used to draw the line of best fit with least squares minimization and predict the optimal drug:polymer ratio.  $x$  represents the drug:polymer ratio, and the constants  $a$ ,  $b$ ,  $c$ ,  $d$ , and  $f$  were optimized with least squares minimization. The function returns the entrapment efficiency.

$$f(x) = (ax^3 + bx^2 + cx + d)/e^{fx} \quad (1)$$

### ACKNOWLEDGEMENTS

We would like to thank the Olive Children's Foundation for providing us with the funding to conduct the research presented in this work. Furthermore, we gratefully acknowledge the Aspiring Scholars Directed Research Program for providing us access to the server to run our simulations on.

**Received:** April 19, 2021

**Accepted:** September 24, 2021

**Published:** January 10, 2022

### REFERENCES

1. Dong, Xiaoxv, *et al.* "Emodin: A Review of Its Pharmacology, Toxicity and Pharmacokinetics." *Phytotherapy Research*, vol. 30, no. 8, 2016, pp. 1207–1218., doi:10.1002/ptr.5631.
2. National Center for Biotechnology Information. "PubChem Compound Summary for CID 3220, Emodin" *PubChem*, <https://pubchem.ncbi.nlm.nih.gov/compound/Emodin>. Accessed 21 August 2021.
3. Fabbro, Doriano, *et al.* "Protein Kinases as Targets for

- Anticancer Agents: From Inhibitors to Useful Drugs.” *Pharmacology & Therapeutics*, vol. 93, no. 2-3, 2002, pp. 79–98., doi:10.1016/s0163-7258(02)00179-1.
4. Aznar, Salvador, *et al.* “Rho Gtpases: Potential Candidates for Anticancer Therapy.” *Cancer Letters*, vol. 206, no. 2, 2004, pp. 181–191., doi:10.1016/j.canlet.2003.08.035.
  5. Kim, R., *et al.* “Effect of Inhibitors of Cysteine and Serine Proteases in Anticancer Drug-Induced Apoptosis in Gastric Cancer Cells.” *International Journal of Oncology*, 2001, doi:10.3892/ijo.18.6.1227.
  6. Kaistha, B P, *et al.* “Key Role of Dual Specificity Kinase Ttk in Proliferation and Survival of Pancreatic Cancer Cells.” *British Journal of Cancer*, vol. 111, no. 9, 2014, pp. 1780–1787., doi:10.1038/bjc.2014.460.
  7. Bhullar, Khushwant S., *et al.* “Kinase-Targeted Cancer Therapies: Progress, Challenges and Future Directions.” *Molecular Cancer*, vol. 17, no. 1, 2018, doi:10.1186/s12943-018-0804-2.
  8. Prieto-Dominguez, Néstor, *et al.* “Drugging the Small Gtpase Pathways in Cancer Treatment: Promises and Challenges.” *Cells*, vol. 8, no. 3, 2019, p. 255., doi:10.3390/cells8030255.
  9. “Polymer Nanoparticle Drug-Nucleic Acid Combinations.” *Nucleic Acids as Gene Anticancer Drug Delivery Therapy*, by Loutfy H. Madkour, Academic Press, 2019, pp. 241–255.
  10. Kamat, Vivek, *et al.* “Chitosan Nanoparticles Synthesis Caught in Action Using Microdroplet Reactions.” *Scientific Reports*, vol. 6, no. 1, 2016, doi:10.1038/srep22260.
  11. Garg, Unnati, *et al.* “Current Advances in Chitosan Nanoparticles Based Drug Delivery and Targeting.” *Advanced Pharmaceutical Bulletin*, vol. 9, no. 2, 2019, pp. 195–204., doi:10.15171/apb.2019.023.
  12. Hou, DongZhi, *et al.* “The Production and Characteristics of Solid Lipid Nanoparticles (SLNs).” *Biomaterials*, vol. 24, no. 10, 2003, pp. 1781–1785., doi:10.1016/s0142-9612(02)00578-1.
  13. Sobhani, Zahra, *et al.* “Nanoparticles of Chitosan Loaded CIPROFLOXACIN: Fabrication and Antimicrobial Activity.” *Advanced Pharmaceutical Bulletin*, vol. 7, no. 3, 2017, pp. 427–432., doi:10.15171/apb.2017.051.
  14. Janeczko, Monika, *et al.* “Emodin, a Natural Inhibitor of Protein Kinase ck2, Suppresses Growth, Hyphal Development, and Biofilm Formation of *Candida Albicans*.” *Yeast*, vol. 34, no. 6, 2017, pp. 253–265., doi:10.1002/yea.3230.
  15. Srinivas, Gopal, *et al.* “Molecular Mechanism of Emodin Action: Transition from Laxative Ingredient to an Antitumor Agent.” *Medicinal Research Reviews*, vol. 27, no. 5, 3 Oct. 2006, pp. 591–608., doi:10.1002/med.20095.
  16. Bank, RCSB Protein Data. “RCSB PDB: Homepage.” RCSB PDB, www.rcsb.org/.
  17. Maust, Joel D., *et al.* “Oncogenic Mutants of mek1: A Trilogy Unfolds.” *Cancer Discovery*, vol. 8, no. 5, 2018, pp. 534–536., doi:10.1158/2159-8290.cd-18-0192.
  18. Sebolt-Leopold, Judith S. “Development of Anticancer Drugs Targeting the Map Kinase Pathway.” *Oncogene*, vol. 19, no. 56, 2000, pp. 6594–6599., doi:10.1038/sj.onc.1204083.
  19. Thorek, Daniel L., *et al.* “Prostate-Specific Kallikrein-Related Peptidases and Their Relation to Prostate Cancer Biology and Detection.” *Thrombosis and Haemostasis*, vol. 110, no. 09, 1 Dec. 2017, pp. 484–492., doi:10.1160/th13-04-0275.
  20. Magnuson, Nancy S, *et al.* “Why Target pim1 for Cancer Diagnosis and Treatment?” *Future Oncology*, vol. 6, no. 9, 2010, pp. 1461–1478., doi:10.2217/fon.10.106.
  21. Yang, Jing, *et al.* “Targeting PI3K in Cancer: Mechanisms and Advances in Clinical Trials.” *Molecular Cancer*, vol. 18, no. 1, 2019, doi:10.1186/s12943-019-0954-x.
  22. Saxton, Robert A., and David M. Sabatini. “Mtor Signaling in Growth, Metabolism, and Disease.” *Cell*, vol. 168, no. 6, 2017, pp. 960–976., doi:10.1016/j.cell.2017.02.004.
  23. Patel, Hitesh, *et al.* “Novel Roles of prk1 and prk2 in Cilia and Cancer Biology.” *Scientific Reports*, vol. 10, no. 1, 2020, doi:10.1038/s41598-020-60604-3.
  24. De, Pradip, *et al.* “Rac1 Takes the Lead in Solid Tumors.” *Cells*, vol. 8, no. 5, 2019, p. 382., doi:10.3390/cells8050382.
  25. Trembley, J. H., *et al.* “Protein Kinase CK2 in Health and Disease.” *Cellular and Molecular Life Sciences*, vol. 66, no. 11-12, 2009, pp. 1858–1867., doi:10.1007/s00018-009-9154-y.
  26. Lee, Shannon, *et al.* “Targeting MAPK Signaling in Cancer: Mechanisms of Drug Resistance and Sensitivity.” *International Journal of Molecular Sciences*, vol. 21, no. 3, 2020, p. 1102., doi:10.3390/ijms21031102.
  27. Xue, Ping, *et al.* “The Aryl Hydrocarbon Receptor and Tumor IMMUNITY.” *Frontiers in Immunology*, vol. 9, 2018, doi:10.3389/fimmu.2018.00286.
  28. Lountos, George T., *et al.* “Structure of Human DUAL-SPECIFICITY Phosphatase 7, a Potential Cancer Drug Target.” *Acta Crystallographica Section F Structural Biology Communications*, vol. 71, no. 6, 2015, pp. 650–656., doi:10.1107/s2053230x1500504x.
  29. Shibuya, Masabumi. “VEGF-VEGFR Signals in Health and Disease.” *Biomolecules & Therapeutics*, vol. 22, no. 1, 2014, pp. 1–9., doi:10.4062/biomolther.2013.113.
  30. Erlejman, Alejandra G., *et al.* “Regulatory Role of THE 90-KDA-HEAT-SHOCK Protein (hsp90) and Associated Factors on Gene Expression.” *Biochimica Et Biophysica Acta (BBA) - Gene Regulatory Mechanisms*, vol. 1839, no. 2, 2014, pp. 71–87., doi:10.1016/j.bbagr.2013.12.006.
  31. Jouandot, David, *et al.* “Functional Dissection of the Glucose Signaling Pathways That Regulate the Yeast Glucose TRANSPORTER GENE (HXT) REPRESSOR RGT1.” *Journal of Cellular Biochemistry*, vol. 112, no. 11, 2011, pp. 3268–3275., doi:10.1002/jcb.23253.
  32. Frenzel, Anna, *et al.* “Bcl2 Family Proteins in Carcinogenesis and the Treatment of Cancer.” *Apoptosis*,

- vol. 14, no. 4, 2009, pp. 584–596., doi:10.1007/s10495-008-0300-z.
33. Bjornsti, Mary-Ann, and Scott H. Kaufmann. "Topoisomerases and Cancer Chemotherapy: Recent Advances and Unanswered Questions." *F1000Research*, vol. 8, 2019, p. 1704., doi:10.12688/f1000research.20201.1.
34. Fernandez-Medarde, A., and E. Santos. "Ras in Cancer and Developmental Diseases." *Genes & Cancer*, vol. 2, no. 3, 2011, pp. 344–358., doi:10.1177/1947601911411084.
35. Tauro, Marilena, and Conor Lynch. "Cutting to the Chase: How MATRIX Metalloproteinase-2 Activity Controls BREAST-CANCER-TO-BONE Metastasis." *Cancers*, vol. 10, no. 6, 2018, p. 185., doi:10.3390/cancers10060185.
36. Huang, Qian, *et al.* "Caspase 3–Mediated Stimulation of Tumor Cell REPOPULATION during Cancer Radiotherapy." *Nature Medicine*, vol. 17, no. 7, 2011, pp. 860–866., doi:10.1038/nm.2385.
37. Battistutta, Roberto, *et al.* "The Replacement of ATP by the Competitive Inhibitor EMODIN Induces Conformational Modifications in the Catalytic Site of Protein KINASE CK2." *Journal of Biological Chemistry*, vol. 275, no. 38, 2000, pp. 29618–29622., doi:10.1074/jbc.m004257200.
38. Hanwell, Marcus D, *et al.* "Avogadro: An Advanced Semantic Chemical Editor, Visualization, and Analysis Platform." *Journal of Cheminformatics*, vol. 4, no. 1, 2012, doi:10.1186/1758-2946-4-17.
39. Trott, Oleg, and Arthur J. Olson. "AutoDock Vina: Improving the Speed and Accuracy of Docking with a New Scoring Function, Efficient Optimization, and Multithreading." *Journal of Computational Chemistry*, 4 June 2009, doi:10.1002/jcc.21334.
40. Quiroga, Rodrigo, and Marcos A. Villarreal. "Vinardo: A Scoring Function Based on Autodock Vina Improves SCORING, Docking, and Virtual Screening." *PLOS ONE*, vol. 11, no. 5, 2016, doi:10.1371/journal.pone.0155183.
41. Suresh, Rohit. "https://github.com/rohits65/activeSiteHeatmap." *GitHub*, 2020, https://github.com/rohits65/activeSiteHeatmap.
42. Schrödinger, LLC. "The PyMOL Molecular Graphics System, Version~1.8." 2015.
43. Vanommeslaeghe, K., *et al.* "CHARMM General Force Field: A Force Field for DRUG-LIKE Molecules Compatible with THE CHARMM All-Atom ADDITIVE BIOLOGICAL Force Fields." *Journal of Computational Chemistry*, 2 July 2009, doi:10.1002/jcc.21367.
44. Van Der Spoel, David *et al.* "GROMACS: fast, flexible, and free." *Journal of computational chemistry* vol. 26,16 (2005): 1701-18. doi:10.1002/jcc.20291
45. Yu, Wenbo, *et al.* "Extension of THE Charmm General Force Field TO SULFONYL-CONTAINING Compounds and Its Utility IN BIOMOLECULAR Simulations." *Journal of Computational Chemistry*, vol. 33, no. 31, 2012, pp. 2451–2468., doi:10.1002/jcc.23067.
46. Vanommeslaeghe, K., and A. D. MacKerell. "Automation of THE CHARMM GENERAL Force FIELD (CGenFF) I: Bond Perception and Atom Typing." *Journal of Chemical Information and Modeling*, vol. 52, no. 12, 2012, pp. 3144–3154., doi:10.1021/ci300363c.
47. Vanommeslaeghe, K., *et al.* "Automation of THE CHARMM GENERAL Force FIELD (CGenFF) II: Assignment of Bonded Parameters and Partial Atomic Charges." *Journal of Chemical Information and Modeling*, vol. 52, no. 12, 2012, pp. 3155–3168., doi:10.1021/ci3003649.
48. Vanommeslaeghe, K *et al.* "CHARMM general force field: A force field for drug-like molecules compatible with the CHARMM all-atom additive biological force fields." *Journal of computational chemistry* vol. 31,4 (2010): 671-90. doi:10.1002/jcc.21367
49. Shen, Jia-Wei, *et al.* "Molecular Dynamics Study on the Mechanism of Polynucleotide Encapsulation by Chitosan." *Scientific Reports*, vol. 7, no. 1, 2017, doi:10.1038/s41598-017-05197-0.
50. Suresh, Rohit. "https://github.com/rohits65/interactionDistances." *GitHub*, 2020, https://github.com/rohits65/interactionDistances.

**Copyright:** © 2022 Suresh *et al.* All JEI articles are distributed under the attribution non-commercial, no derivative license (<http://creativecommons.org/licenses/by-nc-nd/3.0/>). This means that anyone is free to share, copy and distribute an unaltered article for non-commercial purposes provided the original author and source is credited.